Article

Exploration of Key Process Parameters and Properties of 40Cr Steel in Ultrasonic Surface Rolling Process

Xiaobin Wu [1], Jun Cheng [1,2], Zhilong Xu [1,*], Leyang Dai [2,*], Qingshan Jiang [1], Bosheng Su [1], Li Zhu [1] and Zhenye Zhao [1]

[1] College of Marine Equipment and Mechanical Engineering, Jimei University, Xiamen 361000, China
[2] College of Marine Engineering, Jimei University, Xiamen 361000, China
* Correspondence: zhilong.xu@163.com (Z.X.); daileyang@jmu.edu.cn (L.D.)

Abstract: Ultrasonic surface rolling (USRP) is an effective process to improve a workpiece's fatigue property, in which ultrasonic vibration and static force are applied on the workpiece's surface. In order to clarify the ultrasonic rolling strengthening mechanism of critical components and optimize the USRP parameters, a theoretical model of ultrasonic rolling was established. Based on the stress-strain curve of 40Cr steel, the USRP parameters were formulated. The compressive residual stress field of single point impact was analyzed by finite element simulation, and the simulation results were validated by conducting an experimental research. In addition, the changes in the surface properties of specimens under different USRP parameters were studied experimentally. The results show that with the increase in depth, the compressive residual stress on the external surface increases firstly and then decreases, and the maximum compressive residual stress is −338 MPa. As the amplitude is 12 μm and the frequency is 20 kHz, the static force of 600 N is optimal for the ultrasonic rolling of 40Cr steel. This study could provide a guide for the key parameters' selection in USRP.

Keywords: ultrasonic rolling; strain field; residual stress; surface properties

1. Introduction

Numerous discontinuous machining marks appear on the forming surface of critical components, which leads to stress concentration in the service, resulting in a short life and poor reliability [1,2]. In order to improve the comprehensive properties of critical components, many scholars have used traditional surface strengthening processes such as shot peening and mechanical rolling to improve the surface properties. The shot peening process is a kind of cold processing technology. The high-speed mediums impact the workpieces, forming a plastic deformation layer and leaving pits on the surface [3–5]. Mechanical rolling can significantly improve the mechanical properties of specimens, such as the surface hardness, residual compressive stress, and strength and toughness while producing compressive residual stress in the external surface [6]. These processes can improve the surface properties of the specimens and increase their fatigue life to some extent, but their surface performance needs to be improved since the energy density of these processes is not concentrated enough [7,8].

Ultrasonic surface rolling (USRP) is an emerging compound energy processing technology based on traditional mechanical rolling and high-frequency ultrasonic impacts. Ultrasonic impacts cause a certain extent of plastic deformation and strain hardening of the surface microstructure. Hence, USRP can refine the surface grain and produce the compressive residual stress field with a certain depth [9,10]. In comparison with the ultrasonic shot peening, USRP can produce a compressive residual stress and work hardening too. In addition, USRP can obtain a better surface roughness than the ultrasonic shot peening [11]. USRP also has the advantages of being chip free and pollution free, and having a high efficiency, low cost, and good compatibility [12]. Therefore, compared to shot peening and mechanical rolling, USRP is more widely used in improving the surface properties of

components [13–15]. USRP was used to strengthen the 25CrNi2MoV specimens, and the results showed that ultrasonic surface rolling eliminated the surface stress concentration and increased the contact fatigue life of the specimens [16]. Meanwhile, GH4169 superalloy, which has been widely used to manufacture aero engines for high pressure compressors and turbine blades, was strengthened by ultrasonic surface rolling. USRP enhanced the surface hardness of the GH4169 superalloy specimen, decreased the surface roughness, and generated high-intensity compressive residual stress in the surface layer; thus, the fretting fatigue life was increased 11 times [17].

The selection of USRP parameters is a key issue, and the static force has a great influence on the strengthening effect of the specimens. Domestic and foreign scholars have conducted numerous researches on the determination of static force. Li et al. [18] found that the hardness and residual stress on the surface of the specimens increased with the increase in static force after USRP. Wang et al. [19] studied the influence of ultrasonic rolling static force. When the static force was 1100 N, the maximum compressive residual stress could be obtained in the surface layer of a Ti-6Al-4V specimen. However, there have been few researches on the mechanism of ultrasonic rolling surface layer strengthening. All of the above studies were conducted through multiple experiments to determine the optimal static force of ultrasonic rolling.

This paper analyzed the influences of USRP static force on the stress and strain fields of the specimens. According to the stress-strain curve of 40Cr steel, the USRP parameters were formulated. Section 2 analyzed the theoretical model of ultrasonic rolling static force; Section 3 analyzed the compressive residual stress field of a single point impact by finite element simulation; Section 4 analyzed the changes in the surface properties of specimens under different USRP parameters by an ultrasonic rolling experiment.

2. Theoretical Model

In order to determine the parameters of the simulation and experiment, the USRP device was firstly introduced and then the theoretical model of ultrasonic rolling static force was analyzed.

2.1. Description of Ultrasonic Surface Rolling Process

The USRP device mainly consists of a rolling tool tip and ultrasonic wave generator. As shown in Figure 1, the rolling tool tip applies static force and impact force to the specimen surface, and the specimen makes a rotational motion with the spindle. During the USRP, the transducer converts the electrical energy of the ultrasonic generator into mechanical energy and amplifies it through the variable amplitude lever. The rolling tool tip acts on the surface with amplification A along the vertical direction, causing a large elastic-plastic deformation of the specimen, and the surface roughness is reduced. The grain refinement produces a certain hardened layer and compressive residual stress layer, which can inhibit the propagation of fatigue cracks, thus improving the mechanical properties and fatigue properties of the surface layer [20].
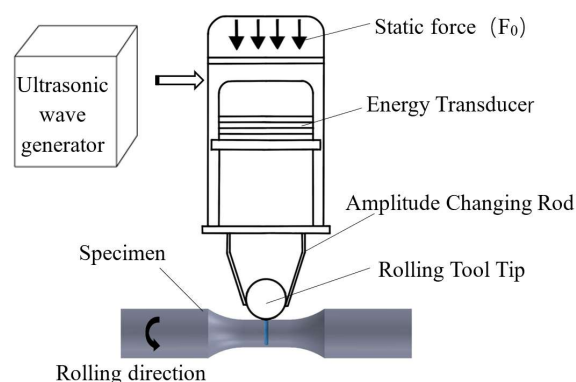

Figure 1. Schematic diagram of ultrasonic surface rolling process.

During the strengthening process, a combined action of static and cyclic longitudinal vibration applied by the rolling tool tip produces impacts on the specimen. The rolling tool tip vibrates in the form of a sine wave. The displacement equation of the rolling tool tip is shown in Equation (1).

$$s = A \sin(2\pi f t) \tag{1}$$

where A is the amplitude; f is the vibration frequency; t is the time.

Taking the derivative of the displacement, we can obtain the equation for the velocity of the rolling tool tip. It is shown in Equation (2).

$$v = \frac{ds}{dt} = 2\pi f A \cos(2\pi f t) \tag{2}$$

Taking the derivative of the velocity, we can obtain the equation for the acceleration of the rolling tool tip. It is shown in Equation (3).

$$a = \frac{dv}{dt} = -(2\pi f)^2 A \sin(2\pi f t) \tag{3}$$

The changes in displacement, velocity, and acceleration of the rolling tool tip are shown in Figure 2. When the displacement of the rolling tool tip was $-A$, the acceleration reached its maximum absolute value, at which time the impact force of the rolling tool tip was the largest. The specimen was subjected to the combined force of the static force and the impact force, and it was at the maximum elastic-plastic deformation. It can be calculated by Equation (4).

$$F = F_0 + F_1 \tag{4}$$

where F is the total force; F_0 is the static force; F_1 is the impact force of the rolling tool tip.
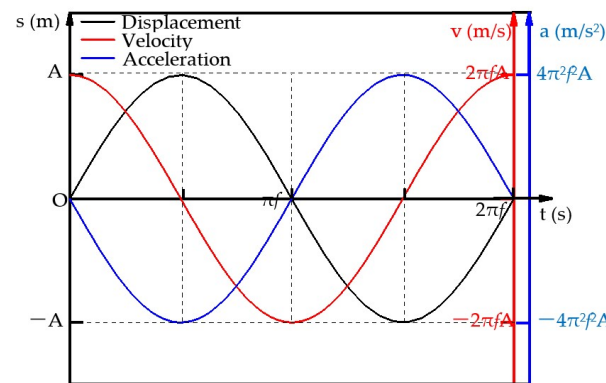

Figure 2. The rolling tool tip movement state.

According to the acceleration equation of the rolling tool tip, the maximum impact force F_1 can be calculated by Equation (5) [21].

$$F_1 = ma = \frac{4}{3}\rho\pi R_1^3(2\pi f)^2 A \tag{5}$$

where m is the mass of the rolling tool tip; ρ is the density of the rolling tool tip; R_1 is the radius of the rolling tool tip.

2.2. Theoretical Model of Ultrasonic Rolling Static Force

During the USRP, the spherical rolling tool tip acts on the external surface of the virgulate specimen. The elastic-plastic deformation region of the specimen is shown in Figure 3. If $\Sigma 1$ is the spherical surface, then $\Sigma 2$ is the specimen surface. The points M and N are the intersection points between the specimen surface and the spherical surface, which are the farthest points of the Y-axis. If R_1 is the radius of the rolling tool tip, then R_2 is the radius of the specimen, and H is the depth of the single point impact pit in USRP. The

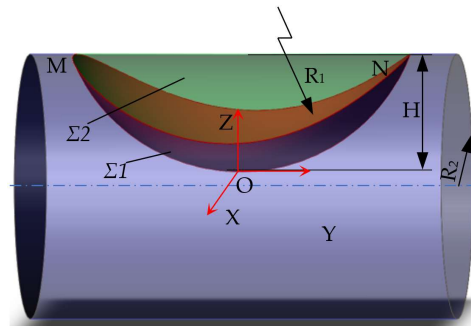Cartesian coordinate system was established with the lowest point of the sphere as the coordinate origin *O*.

Figure 3. Contact deformation area of the specimen.

Based on the Hertz theory, the specimen and the rolling tool tip are assumed to be elastic during USRP. It can be formulated for a contact between two curved elastomers. The relationship between the total force *F* and the maximum depth *H* of the pit can be described as Equation (6) [22].

$$H = \lambda \sqrt[3]{\frac{9A'F^2}{128E^{*2}}} \tag{6}$$

where E^* is the relative modulus of elasticity and it can be calculated by Equation (7); A' and λ are coefficients related to the radius of the specimen and the rolling tool tip, respectively. E_1 is the elastic modulus of the rolling tool tip; E_2 is the elastic modulus of the specimen; μ_1 is the Poisson's ratio of the rolling tool tip, μ_2 is the Poisson's ratio of the specimen [22].

$$\frac{1}{E^*} = \frac{1 - \mu_1^2}{E_1} + \frac{1 - \mu_2^2}{E_2} \tag{7}$$

If the coefficient A' is determined by the radius of the tool tip and the specimen, then it can be calculated by Equation (8).

$$A' = \frac{1}{2}\left(\frac{1}{R_1} + \frac{1}{R_1} + \frac{1}{R_2}\right) \tag{8}$$

λ is the curvature coefficient in Equation (6), and λ is taken by the coefficient θ; it is shown in Table 1.

Table 1. Curvature coefficient value.

θ	0	10	20	30	35	40	45	50
λ	-	0.851	1.220	1.435	1.550	1.637	1.709	1.772
θ	55	60	65	70	75	80	85	90
λ	1.828	1.875	1.912	1.944	1.967	1.985	1.996	2.00

θ can be calculated by Equation (9).

$$\theta = \arccos \frac{R_1}{2R_2 + R_1} \tag{9}$$

According to the Cartesian coordinate system, the equation of the cylindrical surface, $\Sigma 2$, can be described as Equation (10), and $\Sigma 1$ can be described as Equation (11).

$$z = \sqrt{R_2^2 - x^2} + H - R_2 \tag{10}$$

$$z = \sqrt{R_1^2 - x^2 - y^2} + R_1 \tag{11}$$

Since the intersection points M and N are the highest points of the cylindrical surface, their coordinates are M $(0, y_M, H)$, N $(0, y_N, H)$. Substituting it into Equation (11), we can find that $y_M = -\sqrt{R_1^2 - (R_1 - H)^2}$, $y_N = \sqrt{R_1^2 - (R_1 - H)^2}$. Therefore, the range of the deformation region of $\Sigma2$ in the y-direction is $(-\sqrt{R_1^2 - (R_1 - H)^2}, \sqrt{R_1^2 - (R_1 - H)^2})$.

Based on the Hertz contact theory, ignoring the outward extrusion of the specimen material in compression and only considering the vertical compression of the material, h is the value of deformation at each point of the elasto-plastic deformation region, and it can be calculated as Equation (12).

$$h(x, y, z) = \sqrt{R_2^2 - x^2} - \sqrt{R_1^2 - x^2 - y^2} - (R_1 + R_2) + \lambda \sqrt[3]{\frac{9A'F^2}{128E^{*2}}} \tag{12}$$

According to Figure 3, the strain in the elastic-plastic deformation region can be calculated as Equation (13), where α is the correction factor coefficient. Since the deformation of the specimen is very small compared with the original size of the specimen, we introduce the strain calculation coefficient α, which is determined through our previous experiments, and its value is 0.1.

$$\varepsilon = \frac{h}{\alpha R_2} \tag{13}$$

According to Equations (4)–(6) and (13), the maximum strain value in the elastic-plastic deformation region can be obtained as Equation (14).

$$\varepsilon_{\max} = \frac{\lambda \sqrt[3]{\dfrac{9A'\left[F_0 + \frac{4}{3}\rho\pi R_1^3 (2\pi f)^2 A\right]^2}{128E^{*2}}}}{R_2} \tag{14}$$

The ultrasonic rolling static force F_0 can be calculated from Equation (14), therefore it is described as Equation (15). Once the radius of the ultrasonic rolling tip, the radius of the specimen, the material properties of the specimens, and the process parameters of the ultrasonic generator are determined, the static force of USRP can be calculated by the required maximum strain value.

$$F_0 = \sqrt{\frac{128E^{*2}\left[\frac{\alpha R_2 \varepsilon_{\max}}{\lambda}\right]^3}{9\left(\frac{1}{R_1} + \frac{1}{2R_2}\right)}} - \frac{4}{3}\rho\pi R_1^3 (2\pi f)^2 A \tag{15}$$

3. Ultrasonic Rolling Finite Element Simulation

The finite element simulation aims at grasping the laws of the compressive residual stress field in the single point impact of ultrasonic rolling.

3.1. Material Model

The material of the rolling tool tip is cemented carbide (WC) with a hardness of about 3528 HV, and the material of the specimen is tempered 40Cr steel with a hardness of about 322 HV. The stiffness of the rolling tool tip is much larger than the stiffness of the treated specimen, so the rolling tool tip was defined as a rigid body in the ultrasonic rolling simulation. The mechanical properties of both are shown in Table 2.

Table 2. Mechanical performance parameters of material.

Material	Density (kg·m^{-3})	Young Modulus (MPa)	Poisson Ratio	Tangent Modulus (MPa)	Yield Stress (MPa)
40Cr	7.85×10^3	2.06×10^5	0.21	230	785
WC	1.45×10^4	7.10×10^5	0.3	-	-

The plastic deformation of the material in ultrasonic rolling is in a high strain rate state, which belongs to the category of highly nonlinear transient dynamics [23,24]; thus, a combination of dynamic explicit analysis and explicit rebound analysis was used to simulate the plastic deformation and residual stress fields of single point impact on 40Cr steel specimens. Figure 4 presents the finite element model. The rolling tool tip was set to a ball with a radius of 7 mm. The specimen was a round bar with a total length of 100 mm, and the radius of the strengthening area was 4.75 mm. The cell type used to divide the specimen was an eight-node linearly-reduced integration cell (C3D8R). According to the cell size of the equivalent plastic strain, the mesh size of the single-point impact area was set to 0.3 mm, and the model contained 126,741 cells.
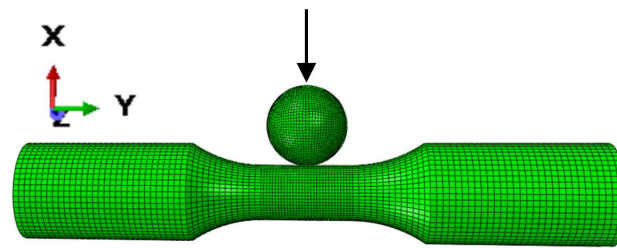

Figure 4. Single point impact finite element model.

During the USRP, elastic-plastic deformation occurs in the specimen surface, which is accompanied by a significant strain hardening phenomenon [25]. Therefore, the effect of strain hardening needs to be considered when choosing the intrinsic model. The Johnson-Cook model assumes that the material is isotropic, and the deformation of materials at strain rates below 10^4 can be described more accurately. The strain rate of the material is in the range of 10^3–10^4 during the USRP [26]. The rolling tool tip completes an impact action for about 5×10^{-5} s. Therefore, in this paper, choosing the Johnson-Cook intrinsic model to simulate the single point impact of USRP is reasonable due to its high accuracy. The expression can be described as follows

$$\sigma = (A + B\varepsilon^n)\left(1 + Cln\frac{\dot{\varepsilon}}{\dot{\varepsilon}_0}\right)\left[1 - \left(\frac{T}{T_0}\right)^m\right] \tag{16}$$

where $\dot{\varepsilon}$ is the plastic strain rate; $\dot{\varepsilon}_0$ is the reference strain rate; T is the temperature; T_0 is the reference temperature; A is the initial yield stress; B is the work-hardening modulus; n is the work-hardening coefficient; C is the strain sensitivity coefficient; m is the temperature sensitivity coefficient, and the specific values are shown in Table 3.

Table 3. Material constants of 40Cr for J-C constitutive model.

Material	*A* (MPa)	*B* (MPa)	*C*	*n*	*m*
40Cr	905	226	0.03	0.26	0.83

3.2. Parameter Settings and Boundary Conditions

Within the ultimate strength of the materials, the compressive residual stress rises as the plastic strain increases, as a result of which, the surface strengthening effect improves [27]. Theoretically, the best strengthening effect is achieved when the strain of ultrasonic rolling is the strain ε_b, corresponding to the ultimate strength of the materials. However, in engineering applications, due to factors such as material uniformity, load fluctuations, and ambient temperature, it is difficult to find the best effect of ultrasonic rolling. Figure 5 shows the stress-strain curve of the 40Cr specimen. The yield strength σ_s of 40Cr is 785 MPa, corresponding to the yield strain ε_s of 0.0038. The ultimate strength σ_b is 980 MPa, corresponding to the ultimate strain ε_b of 0.0495 [22]. In this study, five points, A, B, C, D, and E, were selected near ε_b in order to obtain a better ultrasonic rolling strengthening effect. Their strain values were $\varepsilon_s + 70\%(\varepsilon_b - \varepsilon_s)$, $\varepsilon_s + 80\%(\varepsilon_b - \varepsilon_s)$, $\varepsilon_s + 90\%(\varepsilon_b - \varepsilon_s)$, ε_s,

and $\varepsilon_s + 110\%(\varepsilon_b - \varepsilon_s)$, respectively. These five strain points were targeted for ultrasonic rolling strengthening to analyze the specimen performances. The ultrasonic amplitude was 12 μm and ultrasonic frequency was 20 kHz, the static force corresponding to the five strain points are calculated by Equation (15) and they are shown in Table 4. Both ends of the specimen were completely constrained, and the load of the rolling tool tip was simulated by a combined force of static force and impact force. According to Section 2.1, constant static pressure and sine dynamic impact are applied in the same direction, and the rolling tool tip completes the over frequency vibration impact on the surface of the material while maintaining rolling contact with the surface of the material. The contact between the rolling tool tip and the specimen is set as frictionless contact. The finite element analysis software Abaqus can solve many complex nonlinear problems. Thus Abaqus software (version 2016) was used to simulate the single point impact of USRP.
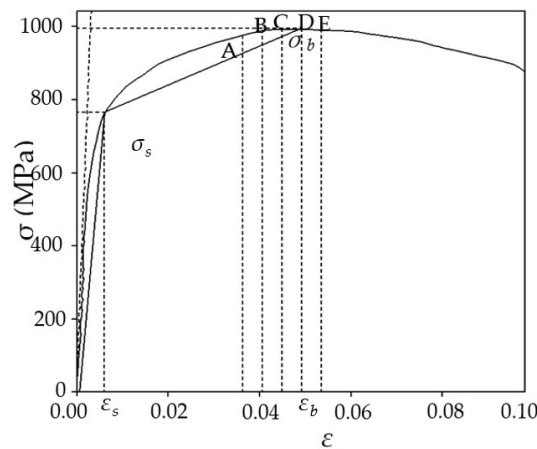

Figure 5. Stress-strain curve of 40Cr material. A, B, C, D and E are points whose strain values are $\varepsilon_s + 70\%(\varepsilon_b - \varepsilon_s)$, $\varepsilon_s + 80\%(\varepsilon_b - \varepsilon_s)$, $\varepsilon_s + 90\%(\varepsilon_b - \varepsilon_s)$, ε_s, and $\varepsilon_s + 110\%(\varepsilon_b - \varepsilon_s)$, respectively.

Table 4. Ultrasonic rolling static force calculation value. A, B, C, D and E are points whose strain values are $\varepsilon_s + 70\%(\varepsilon_b - \varepsilon_s)$, $\varepsilon_s + 80\%(\varepsilon_b - \varepsilon_s)$, $\varepsilon_s + 90\%(\varepsilon_b - \varepsilon_s)$, ε_s, and $\varepsilon_s + 110\%(\varepsilon_b - \varepsilon_s)$, respectively.

Point	A	B	C	D	E
Strain	0.0355	0.0406	0.0454	0.0495	0.0536
F_0 (N)	304	450	600	751	900

3.3. Simulation Results and Analysis

The single point impact of ultrasonic rolling simulation was performed by changing the static force to 300, 450, 600, 750, and 900 N. After the explicit rebound analysis, the plane with the Y-axis as the normal line in Figure 4 was used to intercept the cross section of the specimen and output the stress value from the surface to the interior of the pit center. Then the residual stress distribution along the depth direction is shown in Figure 6. It can be found from the simulation results that there was compressive residual stress on the surface of the specimen, and the compressive residual stress tended to increase firstly and then decrease along the depth direction, finally tending to zero at a depth of about 1 mm from the surface. Figure 6 shows that when the static force was less than 750 N, the maximum compressive residual stress value increased as the static force increased. When the static force exceeded 750 N, the maximum compressive residual stress value decreased as the static force increased. When the static force was 750 N, the compressive residual stress at 200 μm of the subsurface layer was the largest, and its maximum value was −338 MPa. The compressive residual stress in the subsurface was larger than that in the surface, which may be caused by the lack of surface constraint.
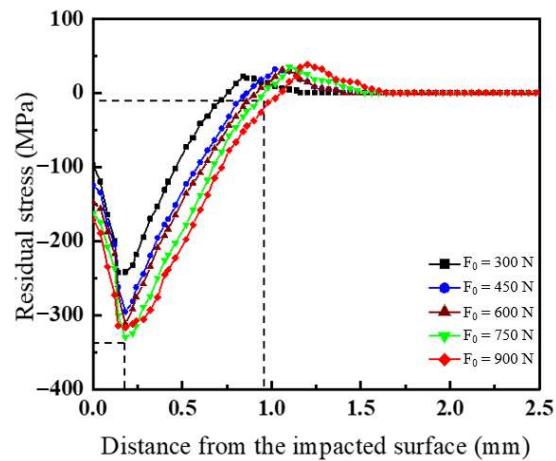
Figure 6. Simulation results of compressive residual stress distribution along the depth.

When the static force was 750 N, the equivalent plastic strain and residual stress distribution on the surface of the specimen at a high strain rate response was obtained. Figure 7a shows that the deformation region of the specimen with single point impact was in the form of an ellipse, and the maximum equivalent plastic strain was 0.049, which occurred at the center of the contact between the specimen and the rolling tool tip. Figure 7b shows the residual stress distribution on the surface of the single point impact deformation region. The compressive residual stress at the center of the contact between the specimen and the rolling tool tip was the largest, and its value was −176.7 MPa. As the distance from the contact center increased, the value of the surface compressive residual stress at each point in the deformation region gradually decreased.
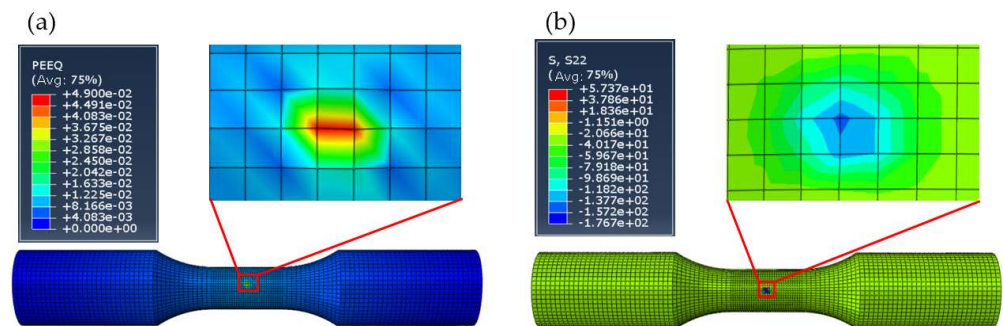

Figure 7. Deformation and stress clouds. (**a**) The equivalent plastic strain; (**b**) residual stress distribution.

4. Ultrasonic Rolling Experiment

4.1. Experimental Equipment and Scheme

The ultrasonic rolling experiment was conducted on HKC30-50 ultrasonic surface rolling strengthening equipment (HuaYun Company, Jinan, China), and the specimens were 20-mm-diameter tempered 40Cr round bars. The chemical composition includes C (0.42%), Si (0.28%), Mn (0.70%), Cr (0.93%), and balance Fe (wt.%). Before the experiment, specimens were finely turned once to ensure the coaxiality between the specimen and the three-jaw chuck of the machine during USRP; then ultrasonic rolling was carried out as shown in Figure 8. According to the calculation results in Table 2, the ultrasonic rolling experiment was set up in 5 groups with different static forces at 300, 450, 600, 750, and 900 N. The ultrasonic amplitude was 12 μm, and the frequency was 20 kHz. The spindle speed was set to 12 rpm, and the specimen was rolled for one turn at a uniform speed.
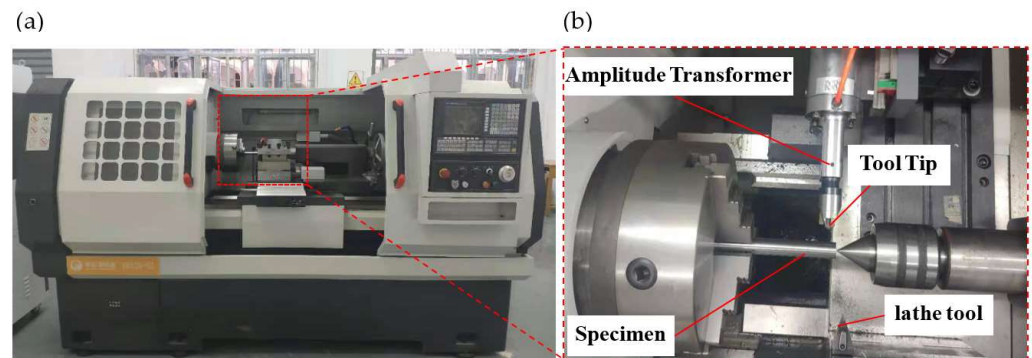
Figure 8. Ultrasonic rolling surface strengthening equipment. (**a**) is the whole equipment and (**b**) is partial enlarged detail.

The morphologies of the rolled grooves after the ultrasonic rolling experiment were observed by a KEYENCE VK-X1000 confocal microscope (Keyence Corporation of America, Broadview Heights, OH, USA); The specimen was corroded layer by layer along the depth direction by electrolytic corrosion method. The residual stress tester HDS-I X-ray (Pulstec Industrial Co., Ltd., Hamamatsu, Japan) was used to measure the residual stress distribution of the grooves by X-ray diffraction method. In order to enhance the reliability of the experimental data, measurements were taken three times for each group, and the average value was taken for analysis.

4.2. Experimental Results and Analysis

4.2.1. Ultrasonic Rolling Groove Morphologies

The specimens were ultrasonically rolled one turn to obtain the rolled grooves, as shown in Figure 9a–e, respectively corresponding to the shape of the rolled grooves for static forces of 300, 450, 600, 750, and 900 N. It was obvious that the amended degree of machining marks on the surface of the specimens increased successively. In Figure 9d, the amended degree of machining marks was the best, while the amended degree of machining marks in Figure 9e had been improved, but there were obvious cracks on the surface of the specimens. Comparing the graphs, it can be seen that the width of the rolled groove increases from 765 to 1205 μm sequentially as the static force increases. Figure 9f shows the comparison between the depth of the rolling groove measured experimentally and the theoretical analysis by Equation (6). From the graph it can be seen that the trend of the two was consistent, the rolling grooves' depth increased with the static force increasing. This is because the stress on the specimen rises as the static force increases, and then the plastic deformation degree enhances. The deviation values of the measured depth and the theoretical depth in the five groups were 11, 13, 11, 14, and 5 μm, respectively. The experimental measured depths were smaller than the theoretical analysis. The reason probably was that the theoretical analysis did not take into account the elastic recovery of the materials. When the static force was 900 N, the static force was larger and the elastic recovery of the materials had less effect on the groove depth, so the experimental measured depth was more similar to the theoretical analysis.

4.2.2. Residual Stress Distribution

During the USRP, the specimen was subjected to high-frequency ultrasonic impact from the rolling tool tip, and the surface material grain refinement and dislocation density increased. After the USRP, the surface layer of the specimens generated compressive residual stress, which can inhibit the expansion of surface cracks and partially offset the tensile stress on the specimen. Compressive residual stress played an important role in improving the fatigue performance of the material. The five groups of 300, 450, 600, 750, and 900 N static force were selected to ultrasonically roll the specimens, and the residual stress distribution along the depth direction is shown in Figure 10a. It can be seen from

the graph that the compressive residual stress tended to increase gradually and then decrease, and the compressive residual stress reached the maximum value −347 MPa, and it was about 170 μm from the surface. According to the Hertz contact theory, the location of maximum contact deformation was in the subsurface layer of the specimen, and the maximum residual stress also appeared in the subsurface layer [28]. The distribution of residual stress in Figure 10a was consistent with the theoretical prediction.
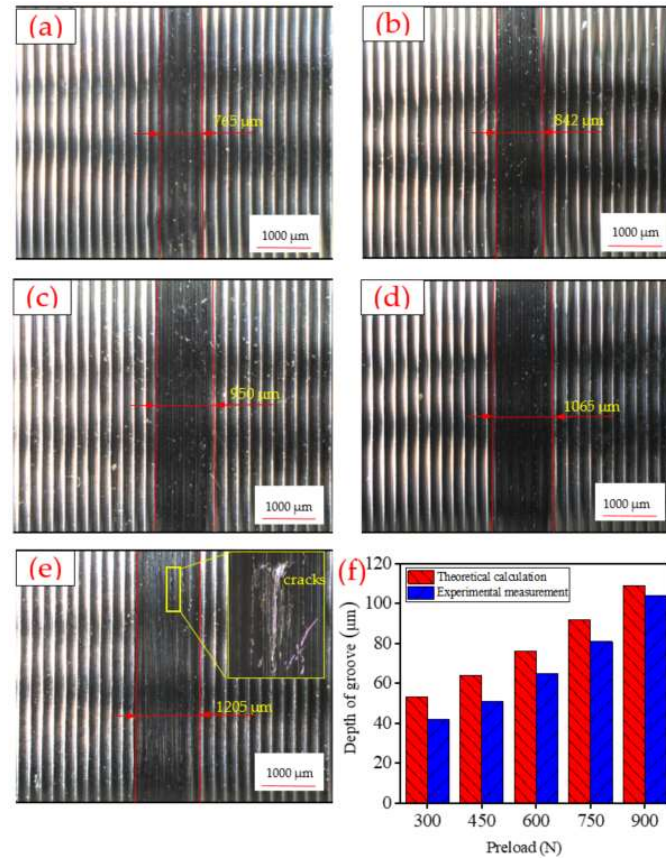

Figure 9. The shapes of ultrasonic rolling grooves. (**a**) Preload 300 N; (**b**) preload 450 N; (**c**) preload 600 N; (**d**) preload 750 N; (**e**) preload 900 N; (**f**) depths of grooves.
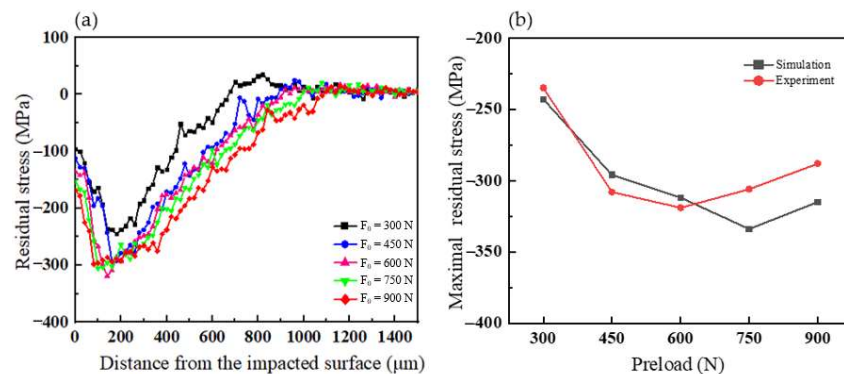

Figure 10. Compressive residual stress distribution after rolling. (**a**) Residual stress distribution along the depth direction in the surface layer; (**b**) comparison of simulation and experimental measurements for maximum compressive residual stress.

The residual stress field of ultrasonic impact was numerically simulated by using the Abaqus software, and the maximum value of compressive residual stress under different static force conditions was obtained. A comparison of the simulated value with the actual experimental measured value is shown in Figure 10b. From the graph, it can be seen that

when the static force was 300, 450, and 600 N, the measured value and the simulated value were approximate. When the static force was over 600 N, the simulated value was greater than the measured value, and the deviation value was about 30 MPa. This could be due to the specimen material's uniformity and the ultrasonic rolling equipment's precision. Then, the major reason for the large deviation between the measured and simulated values was that the Johnson-Cook model adopted in the numerical simulation did not consider the temperature changes during the rolling process. When the static force was less than 600 N, the plastic deformation was small, and the temperature increase was not significant, so there was almost no effect on the value of the residual stress; thus the boundary conditions of the Johnson-Cook model were consistent with the actual, and, therefore, the simulated and measured values were basically the same. When the static force was over 600 N, the plastic deformation was larger and the surface temperature rose obviously, resulting in the relaxation of the residual stress, so the measured value of the compressive residual stress was lower than the simulated value.

According to Equation (16) and Table 2, when the static force was 600 N, the maximum strain value of the specimen was $\varepsilon_s + 90\%(\varepsilon_b - \varepsilon_s)$, and the maximum compressive residual stress value measured along the depth direction was the largest in the five groups of specimens. However, as shown in Figure 6, among the five groups of specimens, the residual stress simulation results showed that the maximum compressive residual stress value was the largest when the static force was 750 N. This was due to the effect of temperature in the simulation being ignored. Combined with the actual measurement data, we can determine that the best static force is 600 N. Therefore, the optimized combination of USRP parameters for tempered 40Cr steel is: the static force is 600 N, the amplitude A is 12 μm, and the frequency is 20 kHz.

5. Conclusions

In the present work, the ultrasonic surface rolling process (USRP) was introduced and the USRP parameters were formulated. Analysis of the experimental observation and numerical simulation results was conducted to characterize the surface layer of materials after USRP. The total investigation can be summarized as follows:

(1) By establishing the mechanical model of USRP, and analyzing the strain field of specimens, the correspondence between the ultrasonic rolling static force and the maximum strain value of the specimens was obtained. When the radius of the ultrasonic rolling tip, the radius of the specimen, the material properties of the specimens, and the process parameters of the ultrasonic generator are determined, the static force of ultrasonic rolling can be calculated by the required maximum strain value. This model can be used for a reference in the selection of ultrasonic rolling static pressure for other materials.

(2) Abaqus software was used to analyze the distribution of the residual stress field for 40Cr specimens after USRP. The compressive residual stress tended to increase firstly and then decrease along the depth direction, and finally tended to zero at a depth of about 1 mm from the surface. When the static force was 750 N, the compressive residual stress at 200 μm of the subsurface layer was the largest, and the maximum value was −338 MPa.

(3) Experimentally, it is concluded that when the amplitude was 12 μm, and the frequency was 20 kHz, the optimal static force of USRP for 40Cr specimens was 600 N. The maximum compressive stress was −347 MPa. The reason for the deviation between the experimental results and the simulation results may be due to the effect of the experimental ambient temperature. Thus in the engineering application, the influences of ambient temperature should be considered during the USRP.

Author Contributions: Conceptualization, Z.X., X.W., Z.Z. and J.C.; methodology, X.W.; software, X.W. and Q.J.; validation, J.C., Q.J. and L.D.; formal analysis, X.W., J.C. and Z.X.; investigation, X.W. and L.Z.; resources, X.W.; writing—original draft preparation, X.W.; writing—review and editing, B.S. and J.C.; visualization, B.S. and Z.X.; project administration, X.W.; funding acquisition, Z.X. and X.W. All authors have read and agreed to the published version of the manuscript.

Institutional Review Board Statement: Not applicable.

Informed Consent Statement: Not applicable.

Data Availability Statement: Not applicable.

Conflicts of Interest: The authors declare no conflict of interest.

References

1. Gao, Y.; Zhao, Z. Surface integrity of gears and the development trend of fatigue-resistant manufacturing technology. *Met. Heat Treat.* **2014**, *39*, 1–6. (In Chinese) [CrossRef]
2. Zerbst, U.; Madia, M.; Klinger, C.; Bettge, D.; Murakami, Y. Defects as a root cause of fatigue failure of metallic components. III: Cavities, dents, corrosion pits, scratches. *Eng. Fail. Anal.* **2019**, *97*, 759–776. [CrossRef]
3. Soyama, H.; Korsunsky, A.M. A critical comparative review of cavitation peening and other surface peening methods. *J. Mater. Process. Technol.* **2022**, *305*, 117586. [CrossRef]
4. Lin, Q.; Liu, H.; Zhu, C.; Parker, R.G. Investigation on the effect of shot peening coverage on the surface integrity. *Appl. Surf. Sci.* **2019**, *489*, 66–72. [CrossRef]
5. Lee, S.; Yu, K.; Huh, H.; Kolman, R.; Arnoult, X. Dynamic Hardening of AISI 304 Steel at a Wide Range of Strain Rates and Its Application to Shot Peening Simulation. *Metals* **2022**, *12*, 403. [CrossRef]
6. Wang, T.; Yang, L.; Tang, Z.; Wu, L.; Yan, H.; Liu, C.; Ma, Y.; Liu, W.; Yu, Z. Microstructure, mechanical properties and deformation mechanism of powder metallurgy AZ31 magnesium alloy during rolling. *Mater. Sci. Eng. A* **2022**, *844*, 143042. [CrossRef]
7. Liu, R.; Yuan, S.; Lin, N.; Zeng, Q.; Wang, Z.; Wu, Y. Application of ultrasonic nanocrystal surface modification (UNSM) technique for surface strengthening of titanium and titanium alloys: A mini review. *J. Mater. Res. Technol.* **2021**, *11*, 351–377. [CrossRef]
8. Ye, C.; Telang, A.; Gill, A.S.; Suslov, S.; Idell, Y.; Zweiacker, K.; Wiezorek, J.M.K.; Zhou, Z.; Qian, D.; Mannava, S.R.; et al. Gradient nanostructure and residual stresses induced by Ultrasonic Nano-crystal Surface Modification in 304 austenitic stainless steel for high strength and high ductility. *Mater. Sci. Eng. A* **2014**, *613*, 274–288. [CrossRef]
9. Dou, Z.; Jiang, H.; Ao, R.; Luo, T.; Zhang, D. Improving the Surface Friction and Corrosion Resistance of Magnesium Alloy AZ31 by Ion Implantation and Ultrasonic Rolling. *Coatings* **2022**, *12*, 899. [CrossRef]
10. Darisuren, S.; Park, J.; Pyun, Y.; Amanov, A. A Study on the Improvement of the Fatigue Life of Bearings by Ultrasonic Nanocrystal Surface Modification Technology. *Metals* **2019**, *9*, 1114. [CrossRef]
11. Safyari, M.; Moshtaghi, M. Role of Ultrasonic Shot Peening in Environmental Hydrogen Embrittlement Behavior of 7075-T6 Alloy. *Hydrogen* **2021**, *2*, 377–385. [CrossRef]
12. Wang, Z.; Xiao, Z.; Huang, C.; Wen, L.; Zhang, W. Influence of Ultrasonic Surface Rolling on Microstructure and Wear Behavior of Selective Laser Melted Ti-6Al-4V Alloy. *Materials* **2017**, *10*, 1203. [CrossRef] [PubMed]
13. Wang, C.; Han, J.; Zhao, J.; Song, Y.; Man, J.; Zhu, H.; Sun, J.; Fang, L. Enhanced Wear Resistance of 316 L Stainless Steel with a Nanostructured Surface Layer Prepared by Ultrasonic Surface Rolling. *Coatings* **2019**, *9*, 276. [CrossRef]
14. Li, G.; Qu, S.; Xie, M.; Ren, Z.; Li, X. Effect of Multi-Pass Ultrasonic Surface Rolling on the Mechanical and Fatigue Properties of HIP Ti-6Al-4V Alloy. *Materials* **2017**, *10*, 133. [CrossRef] [PubMed]
15. Chang, S.; Pyun, Y.; Amanov, A. Wear Enhancement of Wheel-Rail Interaction by Ultrasonic Nanocrystalline Surface Modification Technique. *Materials* **2017**, *10*, 188. [CrossRef]
16. Qu, S.; Hu, X.; Lu, F.; Lai, F.; Liu, H.; Zhang, Y.; Li, X. Rolling contact fatigue properties of ultrasonic surface rolling treated 25CrNi2MoV steel under different lubricant viscosities. *Int. J. Fatigue* **2021**, *142*, 105970. [CrossRef]
17. Yang, J.; Liu, D.; Zhang, X.; Liu, M.; Zhao, W.; Liu, C. The effect of ultrasonic surface rolling process on the fretting fatigue property of GH4169 superalloy. *Int. J. Fatigue* **2020**, *133*, 105373. [CrossRef]
18. Li, F.; Zhao, B. Effect of ultrasonic machining rolling pressure on the surface layer properties of titanium alloy. *Surf. Technol.* **2019**, *48*, 34–40. (In Chinese) [CrossRef]
19. Wang, F.; Men, X.; Liu, Y.; Fu, X. Experiment and simulation study on influence of ultrasonic rolling parameters on residual stress of Ti-6Al-4V alloy. *Simul. Model. Pr. Theory* **2020**, *104*, 102121. [CrossRef]
20. Cheng, M.; Zhang, D.; Chen, H.; Qin, W.; Li, J. Surface nanocrystallization and its effect on fatigue performance of high-strength materials treated by ultrasonic rolling process. *Int. J. Adv. Manuf. Technol.* **2016**, *83*, 123–131. [CrossRef]
21. Li, F.; Zhao, B.; Lan, S.; Feng, Z. Experiment and simulation of the effect of ultrasonic rolling on the surface properties of Ti-6Al-4V. *Int. J. Adv. Manuf. Technol.* **2019**, *106*, 1893–1900. [CrossRef]
22. Liu, Z.; Dai, Q.; Deng, J.; Zhang, Y.; Ji, V. Analytical modeling and experimental verification of surface roughness in the ultrasonic-assisted ball burnishing of shaft targets. *Int. J. Adv. Manuf. Technol.* **2020**, *107*, 3593–3613. [CrossRef]
23. Liu, Y.; Wang, L.; Wang, D. Finite element modeling of ultrasonic surface rolling process. *J. Mater. Process. Technol.* **2011**, *211*, 2106–2113. [CrossRef]

24. Jiao, F.; Lan, S.; Zhao, B.; Wang, Y. Theoretical calculation and experiment of the surface residual stress in the plane ultrasonic rolling. *J. Manuf. Process.* **2020**, *50*, 573–580. [CrossRef]
25. Teimouri, R.; Amini, S. Analytical modeling of ultrasonic surface burnishing process: Evaluation of through depth localized strain. *Int. J. Mech. Sci.* **2019**, *151*, 118–132. [CrossRef]
26. Liu, Y. Research on the Theory and Surface Mechanical Properties of Ultrasonic Rolling Processing on Metal Surfaces. Ph.D. Thesis, Tianjin University, Tianjin, China, 2012. (In Chinese).
27. Geng, J.; Yan, Z.; Zhang, H.; Dong, P. Effect of ultrasonic surface rolling treatment on the organization and properties of AZ31B magnesium alloy. *Surf. Technol.* **2022**, *51*, 368–375. (In Chinese) [CrossRef]
28. Luo, Q.; Zhao, Z.; He, Z.; Li, Z. Contact fatigue failure mechanism of Surface overhardened M50NiL steel. *J. Aeronaut. Mater.* **2017**, *37*, 34–40. (In Chinese)